

Nanoporous Anodic Alumina Platforms for Drug Delivery Applications: Recent Advances and Perspective

Pankaj Kapruwan, Josep Ferré-Borrull, and Lluís F. Marsal*

For several decades, nanoporous anodic alumina (NAA) has been prepared through inexpensive electrochemical anodization of aluminum to prepare diversified periodically ordered nanostructures. It acts as an excellent drug reservoir due to its excellent physical and chemical properties hence minimizing the drug loss and increasing bioavailability to the target site. A rapid increase in exploiting different NAA structures as a drug carrier has been published recently, justifying its potential use in localized drug delivery. In this review, advanced drug releasing structures based on NAA, in vivo and in vitro studies based on their chemical modification, biocompatibility, drug loading, and release kinetics with main focus on recent advances, its progress, and future outlook toward biomedical applications are discussed.

1. Introduction

Drug delivery refers to an approach that either includes formulations or a system that involves infusion of an active pharmaceutical compound inside the body and improves its safe transportation by controlling duration and place of release. An ideal drug delivery system (DDS) is the one where the drug concentration is maximum at the target site and remains constant for a longer time. In earlier times, this was performed with conventional drug delivery methods that included parenteral (injections), oral (pills, tablets, and capsules), or topical formulations (creams and ointments). Nearly a half-century ago, most of the drugs were designed into either capsule or in pill formulations where the drug-loaded inside them used to release immediately upon contact with water without controlling the kinetics.^[1] It was until Folkman et al. in the mid-1960s introduced implantable DDS and first ever zero-order release kinetics study by discovering that the passage of rabbit blood through silicone tubing filled with anesthetic gases makes the rabbit asleep. This experiment successfully laid the foundation of an implant to be used as a drug-mediated carrier. He further added that a drug could replace anesthetic gas and eventually, it would release the drug at a constant rate as well.^[2] Unfortunately, conventional drug delivery therapies require multiple

dosages to maintain drug level in the body and there is usually a rapid release of the drug directly into the blood circulation within a short time before reaching the desirable site, which might possess a risk of damaging healthy organs.^[3] The main problem with these types of delivery vehicles includes poor patient compliance, lack of selectivity, unavoidable drug solubility, and biodistribution along with unfavorable elution kinetics.^[4]


With recent advances in nanofabrication technologies, drug delivery systems have achieved a significant progress in terms of patient safety, bioavailability, and achieving required therapeutic effi-

ciency.^[5,6] Two new branches, i.e., localized drug delivery systems (LDDSs) and targeted drug delivery systems (TDDSs) have emerged to efficiently deliver a drug inside the body using many nano-based drug carriers. These carriers include nanoparticles, liposomes, dendrimers, micelles, nanospheres, nanotubes, graphene.^[7–11] Both of these concepts have already been executed in clinical practices performing excellently in terms of cost-effectiveness, less painful technologies, controlled and reliable drug release profile.^[12]

Amidst different categories of nanomaterials developed for drug release, inorganic nanoporous structures are the center of attraction for most of the researchers today due to its ease of fabrication, cost-effectiveness, and ability to tune structural parameters precisely.^[13] In recent years, nanoporous anodic alumina (NAA), porous silicon (pSi), and titania were thoroughly investigated among all nanoporous materials specifically for developing new drug-releasing strategies due to their excellent physiochemical properties and biocompatible properties.^[14–16] Among all the materials mentioned above, NAA remains one of the best choices due to its excellent chemical inertness, biocompatibility, enhanced mechanical strength, tunable chemistry, and controlled pore dimensions and volumes for loading and releasing drugs in a controlled manner.^[14,17–20] In addition to its biomedical importance, NAA is also being utilized in optical biosensing, energy production, and catalytic applications.^[13,21–25]

This review compiles the most recent advances in NAA platforms for drug delivery applications with a short introduction for efficient drug delivery strategies developed over the years. To start with, the fundamental fabrication process, their properties, and biocompatibility of NAA are briefly introduced. The main intention is to summarize the different nanostructures based on NAA currently being developed for drug delivery applications, their advantages, and limitations. Furthermore,

P. Kapruwan, Dr. J. Ferré-Borrull, Prof. L. F. Marsal
Departament d'Enginyeria Electrònica
Elèctrica i Automàtica
Universitat Rovira i Virgili
Avinguda Països Catalans 26 43007, Tarragona, Spain
E-mail: lluis.marsal@urv.cat

 The ORCID identification number(s) for the author(s) of this article can be found under <https://doi.org/10.1002/admi.202001133>.

DOI: 10.1002/admi.202001133

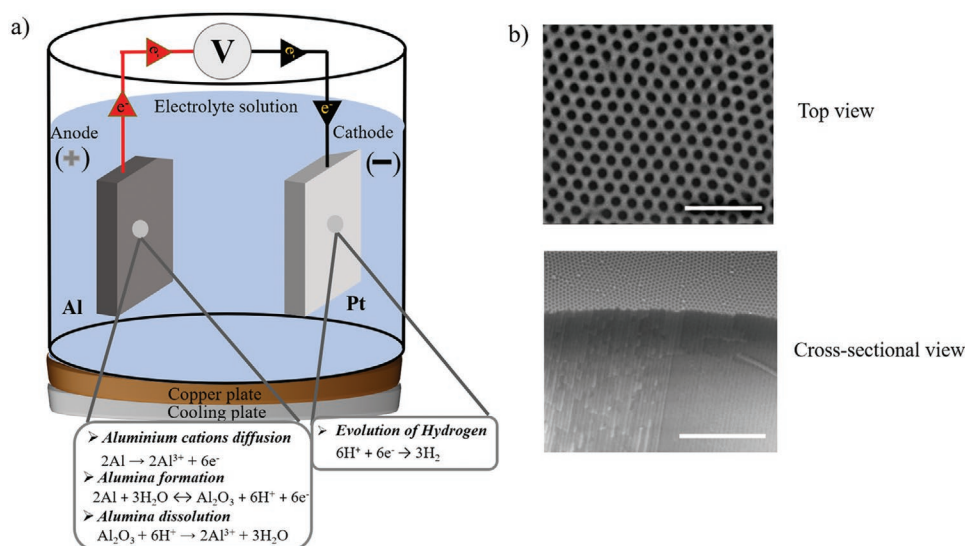


Figure 1. a) Fabrication process of nanoporous anodic alumina using an electrochemical setup. b) ESEM top and cross-section view (scale bars = 500 nm and 3 μm, respectively). Inset shows the chemical reaction occurs during anodization.

the details have been elaborated about recent progress with in vivo and in vitro studies for biomedical applications. Finally, a general overview with the future prospective outlook on recent trends in this field has been concluded.

2. Nanoporous Anodic Alumina: Fundamentals, Structure, and Properties

NAA is fabricated by simple electrochemical anodization of aluminum and consists of closely packed hexagonal arrays of nanopores from top to bottom obtained during anodization (Figure 1). Despite many research activities carried out in recent years, a complete explanation of self-organization process still needs to be validated. However, many studies have proved that the self-organization mechanism occurs primarily due to two reasons, the first one being the field-assisted dissolution of alumina layer at the interface of oxide/electrolyte, whereas the second reason includes localized stress between neighboring and growing nanopores at the interface of metal/oxide which results in a process of self-organization in the hexagonal form to reduce mechanical stress.^[26]

Although NAA production has been widely used in the metal finishing industry for a long time, remarkable progress toward NAA fabrication with exceptionally good pore ordering was achieved by Masuda and Fukuda,^[27] which revolutionized this material growth to a great extent. Their simple electrochemical approach uses a two-step anodization procedure toward the fabrication of highly ordered nanostructures based on the self-ordering phenomenon. Geometrical characteristics such as pore dimensions, size, shape, interpore distance, and length can be controlled by varying anodization voltage, type, electrolyte concentration, and temperature.^[14] This opens up a broad range of possibilities to fabricate pore structures ranging from diameters as low as 5 nm to a few hundred nanometers. The pore length can also be tuned from tens of nanometers to a hundred micrometers by modulating the etching time.

This lithography-free approach consists of two anodization steps where the resulting oxide layer obtained from the first step is chemically removed to obtain hexagonal patterns on the aluminum substrate. The second anodization step is performed afterward under the same conditions as the first one and results in the self-organized growth of cylindrical nanopores from top to bottom. This type of anodization usually happens at low voltages and is referred to as “mild anodization” (MA). The process is primarily performed in three different types of electrolytes, i.e., sulphuric,^[28] oxalic, and phosphoric^[29] followed by other kinds of acids such as malonic^[30] or citric.^[31] Usually, the oxide growth rate for MA is low and range between 3 and 8 μm h⁻¹. Henceforth, another regime, known as hard anodization (HA) was introduced by Lee et al.,^[32] which is performed at high voltage and low electrolyte temperature that offers high oxide growth rate between 50 and 70 μm h⁻¹.^[33] NAA prepared through this approach possesses intrinsic biocompatibility, relatively high surface area and porosity, excellent physiochemical properties, which act as a perfect reservoir for loading and releasing of active drug (Figure 2a–f). Apart from the routine anodization strategies mentioned above, there are several other types of modified anodization processes that can be applied to obtain more complex structures. Details can be found in Table 1 below.

Exploring this approach, researchers worldwide have developed several nanoplatforms based on NAA to address several medical problems.^[8]

With its high pay loading capacity and excellent homogeneous ordered structure, it serves as one of the excellent candidates for drug loading and release as compared to other porous structures.^[46,47] Due to its tremendous properties including mechanical robustness, lightweight, bioinertness, and corrosion resistance, it is widely used for fabricating different templates,^[48] which can be tailored into different shapes (nanotubes, nanowires, nanoneedles, etc.) without the usage of heavy equipment and hazardous chemicals that favors mass production at industrial level. Taking advantage of these properties, several research groups have reported the encapsulation

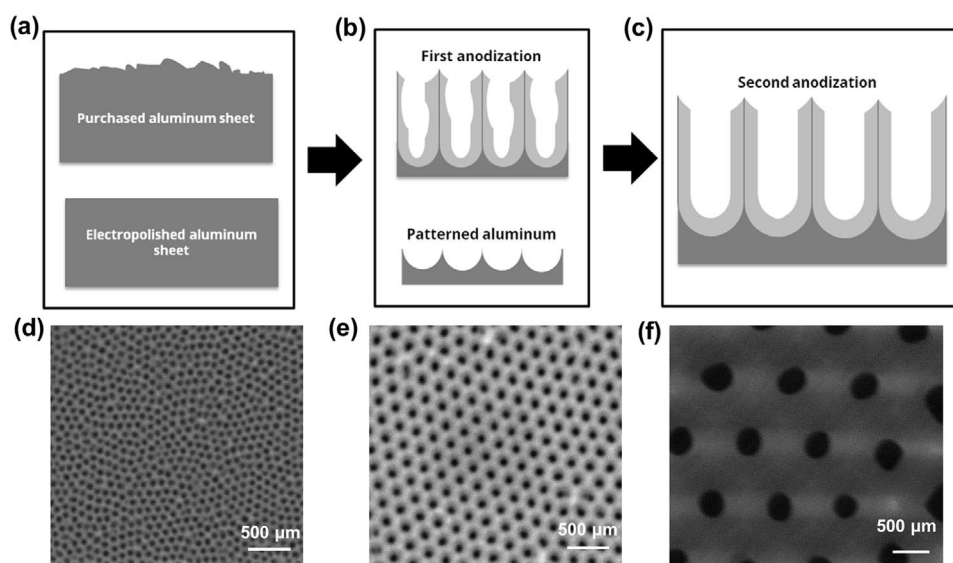


Figure 2. Schematic of NAA structure fabricated by electrochemical anodization following the two-step anodization process. a) As-purchased aluminum sheet followed by electropolishing treatment to decrease surface roughness. b) First step depicting starting of nucleation process, which is further chemically treated to remove sacrificial oxide layer. c) Second step anodization to obtain desired oxide thickness. d,e) ESEM image of as-produced NAA top view in d) sulphuric, e) oxalic, and f) phosphoric acid, respectively. Adapted with permission.^[49] Copyright 2016, Springer.

of drug carriers, small molecules with different functionalities, micellar structures and to some extent large molecules as well including DNA, RNA, and proteins.^[20,33] Diffusion-controlled release profile can easily be obtained by structural modification of NAA by varying pore dimensions and length.^[48] Typically, the process is controlled by several factors, i.e., porosity and length, diffusion coefficient, the molecular size of drug, surface functionalities on the pores, etc. There are different types of release profiles that can be obtained from NAA, which includes burst release, zero-order, first and second-order combined, or stimuli-based drug release.^[49,50] However, among all, zero-order release is considered as one of the best release profiles as it resembles the drug release at a constant rate independent of concentration and time. In addition to the release profiles mentioned above, NAA also serves as an excellent drug carrier for generating other types of drug release profiles for instance, smart and on-demand, sustained, switchable behavior thus reaching one step closer to smart drug delivery applications.

3. Biocompatibility of NAA

Several studies have demonstrated that biomaterials arouse the immunological response of the body, which alters their functional properties and action mechanisms.^[51,52] Therefore, biocompatibility is one of the utmost parameters required for any biomaterial before its usage in real-life clinical practices. Alumina (Al_2O_3) is a highly insoluble, nontoxic material widely used in dental and orthopedic treatments due to its bioinertness and excellent resistance.^[53] The fabrication process of NAA does not require any heavy equipment and thus safe to use. Some of the best uses of NAA are focused on their real-life clinical applications as implants, tissue, and stem cell engineering due to their high surface area, chemical stability, excellent topography, and high wettability. Enormous research activities have been carried out to understand the behavior of NAA with different cell lines and tissues that include neuronal, connective tissue, epithelial, muscular, and blood cells.^[54–61]

Table 1. Classification of different anodization processes used for fabrication of NAA.

Architectures	Anodization	Electrolyte	Refs.
Anodic alumina nanotubes	Pulse anodization	• 0.3 M H_2SO_4	[34–36]
Funnel-like structures (normal and inverted)	Modified anodization approach	• H_3PO_4	[37,38]
Multilayered (DBRs, GIFs, $\mu\text{-CV}$)	Stepwise pulse anodization (STPA), pseudosinusoidal anodization	• 0.3 M $\text{H}_2\text{C}_2\text{O}_4$ • 1.1 M H_2SO_4 with 25% ethanol • 0.3 M oxalic acid ($\text{H}_2\text{C}_2\text{O}_4$)	[39–42]
Hierarchical	Asymmetric two-step anodization	• 0.1 M H_2SO_4 • 0.2 M $\text{H}_2\text{C}_2\text{O}_4$ • 0.3 M H_3PO_4	[14]
Serrated nanochannels	Anodization approach using low voltage and high temperature	• 6 wt% aqueous phosphoric acid	[43]
Modulated	Alternating MA and HA conditions	• H_3PO_4	[44,45]

These studies prove that NAA offers excellent biocompatibility and does not provide a threat to neighboring cells/tissues and at the same time providing good cell attachment.

3.1. In Vitro Biocompatibility Studies

Extraordinary research to explore NAA in drug delivery studies was performed by Desai et al. where the team studied thoroughly NAA capability as cellular encapsulation to release immunoglobulin (IgG), glucose, and insulin. In this work, biocapsules consisting of nanoporous alumina membranes were developed using aluminum tubes as substrates. The potential use of these implantable biocapsules as an alternative treatment for type 1 diabetes was investigated. Pore sizes of 46, 58, and 75 nm were obtained using two-step anodization processes and filled with insulin-secreting MIN6 insulinoma cells placed within a collagen matrix. Results showed the glucose molecules were actively released, while, IgG release was significantly obstructed. Considerably, it was noted that the lack of nutrition inside the structure influenced the release of insulin. Results indicated that the release of insulin from these NAA biocapsules continued for up to 3 h suggesting that the encapsulated cells were able to produce new insulin.^[62,63]

In another study by Karlsson and Tang, NAA membranes were prepared and subsequently coated with collagen I, serum, fibrinogen, IgG, and albumin to study in vitro cell viability of osteoblastic cells (MG63). Pore size-dependent responses were observed on protein-coated NAA membranes. Highest response in cell numbers was noticed when NAA membranes (20 and 200 nm pore size) were incubated with collagen I. On the other hand, cells cultivated on fibrinogen-coated membrane were found to be more viable on 20 nm as compared to 200 nm structure, the reason for this was attributed to the physical characteristics, i.e., size and shape of fibrinogen. It was also reported that albumin has more binding affinity to this substrate than IgG.^[58]

Pujari-Palmer et al. found that the nanotopographic surface of NAA has a significant impact on bone cells behavior. NAA membranes with different pore diameters (20, 100, and 200 nm) and 60 μm thickness were taken in the study and tested for their osteoinduction and drug delivery kinetics. For cell growth study, Bone marrow stromal cell lines (W20-17) were used and cultured on these nanoporous anodic alumina membranes. Alkaline phosphatase (ALP) expressions were measured to analyze the effect of different pore sizes on osteogenic differentiation in stromal cell lines. The potency of NAA to release an osteoconductive agent—bone morphogenic protein-2 (BMP-2) was also reported alongside. Also, an in-depth analysis was conducted based on the mechanism of cell proliferation, gene expression. The interaction of nanopores with cells has been depicted in **Figure 3a,b** where different cell morphology grown on different pore diameters (20 and 200 nm) are shown. On one hand, NAA membranes with a pore diameter of 20 nm were flat and round shape, membranes with 200 nm were found to be in an elongated form. In **Figure 3c**, it is shown that the rate of cell proliferation was found to be more on the control surfaces as compared to NAA surfaces when analyzed with Alamar blue assay (**Figure 3d**). Not much

significant differences were observed between alumina and control samples considering the proliferation rate among different pore diameters; **Figure 3e** shows higher ALP activity in cells on 200 nm membranes as compared to 20 and 100 nm membranes after 14 days culture. In terms of differentiation rate, **Figure 3f** shows that the differentiation rate was higher on the 200 nm membrane as compared to 100 nm membranes without the addition of BMP-2 protein. No significant difference was observed for all the surfaces with the BMP-2 addition (**Figure 3g**); osteocalcin (OC) gene expression was found to be on the higher side on 200 nm membranes compared to 20 nm surfaces and the same pattern was observed when the cells were treated with BMP-2.^[64]

3.2. Cell Attachment on NAA Surfaces

Surface topography of NAA has attracted much attention in recent years with many exciting research outputs put forward by the researchers in terms of an interaction between different cell lines and nanostructures surface. This, in turn, has enabled the development of new methods for enhanced cell culture processes with the possibility of deep understanding between cell adhesion, behavior, and differentiation with regards to NAA surfaces.

Titanium implants covered with a layer of anodic aluminum oxide (AAO) were prepared by Walpole et al. where aluminum was deposited on to titanium alloy and subsequently anodization was performed in 0.4 M phosphoric acid. The alumina layer was bonded to the titanium substrate via an interfacial layer consisting of dense anodized titanium oxide. To validate the coating process, mechanical measurements were performed to calculate shear and tensile strength, which was found to be more than 20 and 10 MPa, respectively. The biocompatibility of this implant was examined against osteoblastic activity and its phenotype. It was observed that AAO surface provides an excellent surface for osteoblast cell growth but on the other hand, the osteoblastic phenotype was retained. To analyze the dissolution rate, AAO was placed in cell culture medium along with the growing cells. It was found that after 9 days of incubation, membrane lost only 0.03% of their weight which is far below the toxic level. Enhanced biological performance was also reported by filling the porous structure with colloidal silica particles having a size of 20 ± 4.8 nm.^[65]

Hoess and co-workers^[66] found that by cultivating hepatocytes cell line HepG2 on NAA membranes, good cell growth conditions were obtained. The membranes were prepared to have pore diameters of 70 and 260 nm. Cell culture experiments demonstrated that the cells showed excellent proliferation and adhesion on the NAA membranes for up to 4 days with normal morphology and no signs of toxicity. In addition, filopodia were found penetrating inside the larger pores with a diameter of more than 200 nm. The biomedical capability of NAA was tested against Vero cell lines, which belong to the kidney of *Cercopithecus aethiops* (African green monkey).^[67] Cell adhesion studies were conducted with in-house prepared NAA membranes, commercially available Whatman Anopore (Anodisc) membranes, and glass slides. **Figure 4a–c** shows optical characterization after 24 h of cell interaction with all

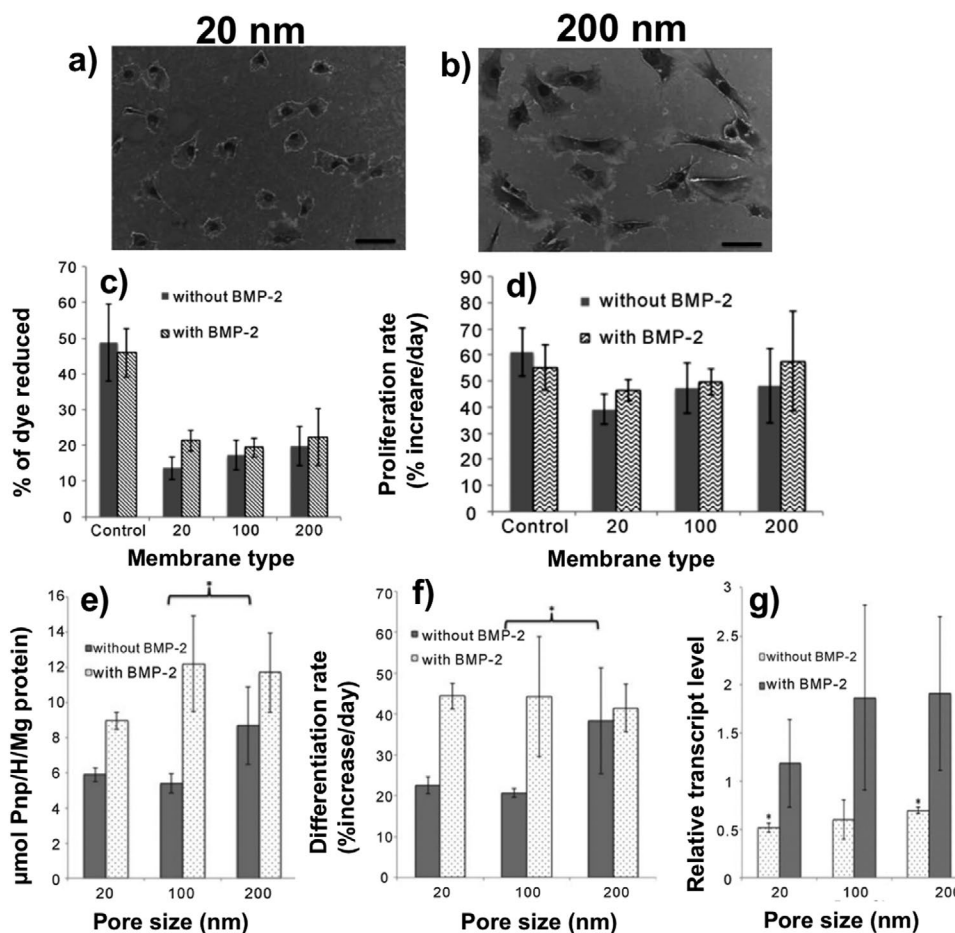


Figure 3. W20-17 cell morphology after cell culturing for 2 days on a) 20 nm and b) 200 nm. c) Alamar blue assay profile of proliferated cells after 7 days. d) Day wise analysis of increase in cell number from 2 to 7 days. e) Alkaline phosphatase (ALP) activity after 14 days of cell culture, with polystyrene as a control and NAA (20, 100, and 200 nm), with and without addition of BMP-2. f) Measurement of cell differentiation rate by analyzing increase in ALP activity by time (12 days) from day 2 to day 14. g) OC gene expression with and without BMP-2 was analyzed at 14 days. Adapted with permission.^[64] Copyright 2014, Scientific Research Publishing.

the substrates. In Figure 4d–f, field emission scanning electron microscopy (FESEM) images showed the presence of filopodia over the entire NAA surface, generating extracellular matrix (ECM) actively. It was reported that for the duration of the 72 h period, the cell proliferation rate was less for those cultured on glass slides as compared to porous substrates. Also, there were no signs of any toxicity on the cells. To confirm Vero cell viability, cell proliferation assay was performed represented in Figure 5a. It was found that at the end of 72 h, both the types, i.e., Anopore and in-house NAA membranes were superior in terms of cell viability as compared to glass control (Figure 5b).

In another study, to assess the proliferation and attachment of preosteoblast (MC3T3-E1) cell lines, Ni et al. fabricated NAA of different pore structures with pore diameters varying between 25 and 70 nm. It was found that after cultivating the cells for 7 days in a culture medium, at the beginning moderate differences were observed in preosteoblast attachment whereas the proliferation rate was found to be dramatically increased at the larger pore sizes, i.e., 50 and 75 nm. It was reported that enhancing the osteoblast density on the aluminum surface can be achieved by improving the surface roughness only and

without any change in chemistry.^[68] To study the importance of pore depth, Thakur et al. studied the living cells (vascular endothelial cells (ECV 304) response on PAA surface. The cells were cultured on the nanoporous surface and after 1 day treated with polymerized actin in the presence of 3.7% formaldehyde. It was reported that for shallow pores (50 and 200 nm pore depth), the cells were found to be round with the presence of actin in an amorphous form throughout the cytosol distribution with no major differences. However, on deep pores (2000 nm), the cells morphology and its arrangement in its cytosol compartment solely depends upon the pore size.^[69]

To test the biocompatibility of different NAA structures, Wang et al. fabricated 600 nm long anodic alumina nanotubes (AANTs) through pulse anodization and conducted cytotoxicity experiments using Alamar blue and crystal violet assays.^[70] Different concentrations of AANTs (1.56 – $100 \mu\text{g mL}^{-1}$) were obtained for toxicity experiments carried out for 1–5 days on breast cancer cells (MDA-MB231-TXSA) and macrophage cells (RAW264.7). It was demonstrated that even after 5 days, no toxicity patterns were observed in both the cell lines indicating that NAA tubes did not have any negative impact on

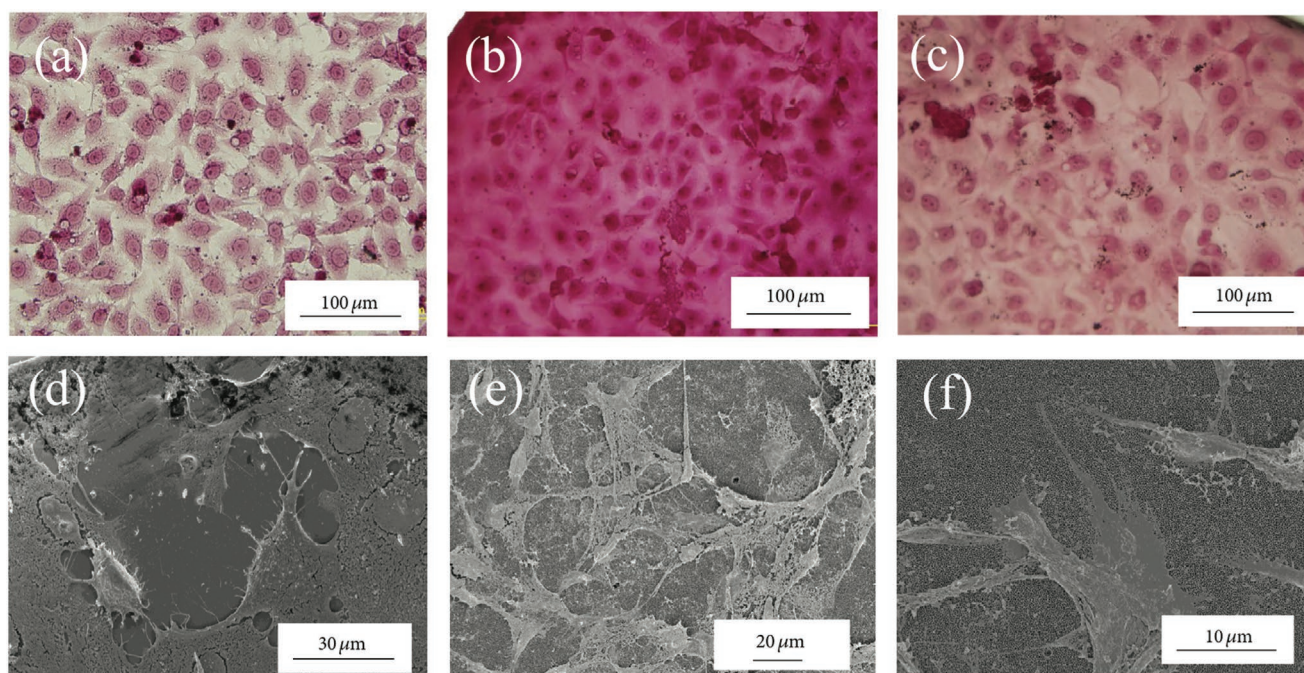


Figure 4. Optical characterization of Vero cells a) glass, b) Whatman membrane, and c) NAA in-house membrane, and FESEM images at different magnifications d) glass, e) Whatman membrane, f) NAA in-house membrane. Adapted with permission.^[67] Copyright 2014, Hindawi.

cell growth and morphology (Figure 6a–f). To see the interaction between AANTs and cell lines, transmission electron microscopy (TEM) examination was carried out as depicted in Figure 6g,h. NAA tubes were seen inside the RAW264.7 cells where bonding of autophagosome with autophagic can clearly be seen within the area highlighted. These results successfully demonstrate the uptake of AANT inside the cell. In a similar manner, another study was carried out with AANTs having lengths of 0.7, 2.5, and 5.8 μm fabricated through pulse anodization process. It was shown that all three different types of AANTs fabricated were taken up by the cells, however, AANTs with the length of 0.7 μm shows the lowest toxicity among all.^[35]

3.3. In Vivo Biocompatibility Studies

Most of the research conducted using NAA as a template involves in vitro experiments, but when it comes to real-life applications, more in vivo and in-depth studies are required, which present deep challenges.

In these regards, Wieneke et al. studied the effect of NAA coating on stents as a potential carrier for the delivery of the tacrolimus drug. In this study, 316 L stainless steel stents were covered with a thin layer of NAA followed by infiltration of 60 and 120 μg of the drug. Bare stents, coated stents, and a drug-loaded coated stents were fabricated and implanted in the carotid artery of New Zealand white rabbits. Drug release was

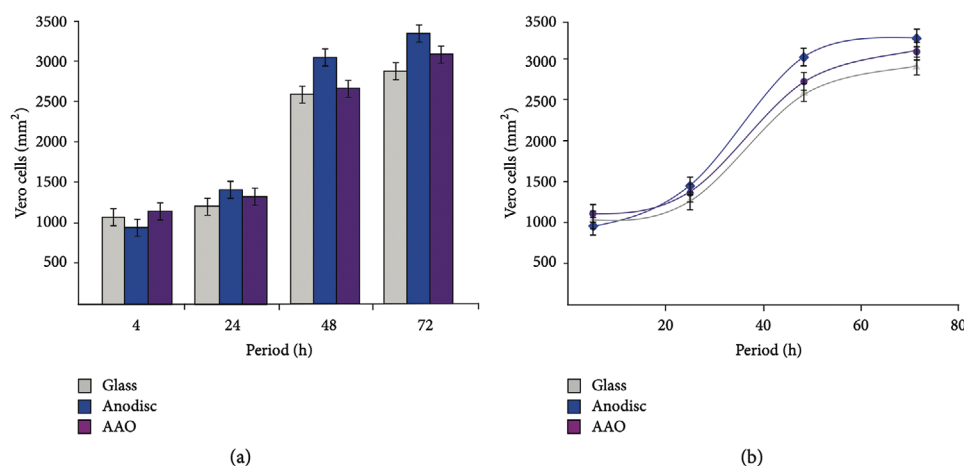


Figure 5. a) Vero cell proliferation study on three substrates after 72 h; b) comparison of Vero cell count against different substrates. Adapted with permission.^[67] Copyright 2014, Hindawi.

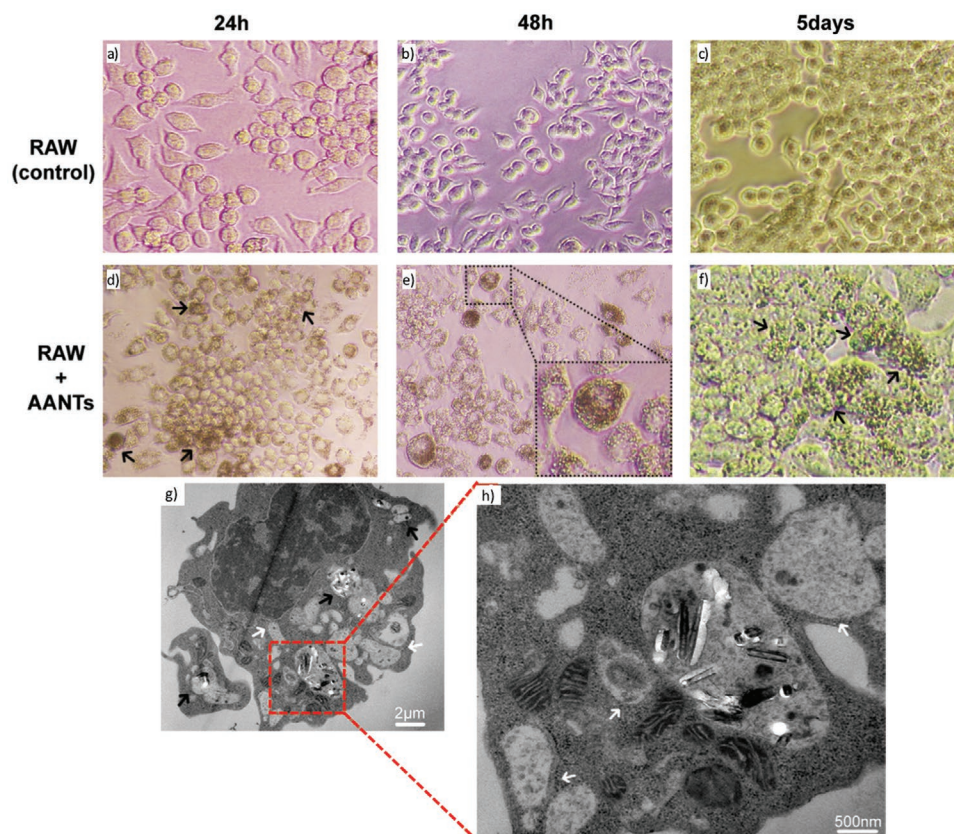


Figure 6. Optical characterization of AANTs ($100 \mu\text{g mL}^{-1}$) after incubation with RAW 264.7 cell lines a,d) 24 h, b,e) 48 h, and c,f) 5 days. Black arrows in (d)–(f) show that the cell is surrounded by AANTs along with the darker spot on the cells due to light refraction of alumina. g) TEM picture of internalized NAATs ($100 \mu\text{g mL}^{-1}$) by RAW 264.7 macrophage cell with white arrows denoting the blending of autophagic vacuoles h) enlarged view. Adapted with permission.^[70] Copyright 2014, Elsevier.

monitored by extracting whole blood at different time intervals and measuring with HPLC. It was shown that NAA-coated stents served as an excellent platform for loading and release of drug within therapeutic range followed by a significant reduction in neointima thickness.^[71]

Rahman et al. demonstrated a novel method for ex vivo drug release in bones using the Zetos bioreactor (Figure 7a–g).^[72] NAA implants with pore diameter (30–35 nm) and depth of 10–60 μm were fabricated. These NAA wires impregnated with rhodamine B (RB) dye were placed directly into the bone using needle puncture procedure and drug elution kinetics was measured by live fluorescence imaging. Biocompatibility study was also performed using human osteoblast cells, which responded with strong growth and adhesion to the NAA surface. Histology examination reveals the presence of live osteocyte cells along with an insertion area demonstrating the harmlessness of the device to adjacent areas what makes the system suitable for clinical practice. In addition, this approach did not have any impact on NAA and surrounding bone cells (Figure 8a–d). Different concentrations of drug profiles in bone were achieved, which showed the distribution of drug molecules from NAA implants in all directions. The results showed that by controlling pore length it is possible to obtain an extended drug release profile (Figure 8e).

4. Structural and Surface Modifications

Surface functionalization of NAA is limited due to the presence of oxides along with some other impurities caused by the preparation process.^[73] One of the best strategies to overcome this limitation is to modify the surface by introducing different functional groups to improve the overall physiochemical properties of NAA.

Some of the best methods to modify the surface with different strategies and materials has been listed in Table 2 below.

The techniques mentioned above have been widely tested successfully over time. One of the easiest approaches developed over the years is to control drug delivery by modifying the pore dimensions and fabricating different types of nanostructures based on NAA.^[37,70] In 2003, Gong et al.^[95] fabricated mechanically robust tubular NAA membranes of different pore sizes (25–55 nm) using aluminum microtubes as substrate and applying the two-step anodization process in 0.2 M oxalic acid. To conduct diffusion experiments, these tubular membranes were transformed into filtration capsules loaded with two different types of molecules (used to model the elution dynamics) such as fluorescein (small size) and fluorescein isothiocyanate (FITC)–dextran with different molecular weights to study the drug release profiles as a function of pore size. Results showed

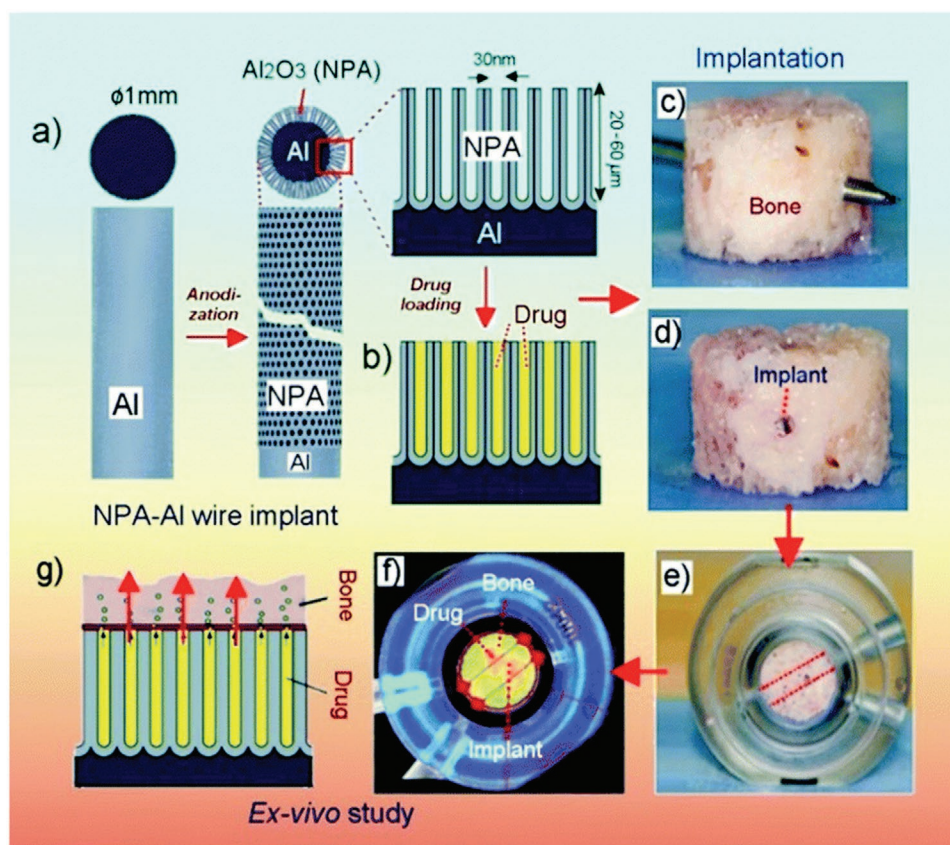


Figure 7. a–g) Schematic of fabricated and drug-loaded NAA implant insertion into ex vivo bone model and in situ fluorescence drug elution kinetics. Adapted with permission.^[72] Copyright 2015, Royal Society of Chemistry.

that fluorescein release followed Fickian diffusion and was released within a couple of hours. On the other hand, for FITC-dextran, that follows Knudsen diffusion, no noticeable drug

diffusion was observed despite having a low hydrodynamic diameter (11.6 nm) as compared to pore diameter (55 nm). The reason was attributed to the fact that supramolecular

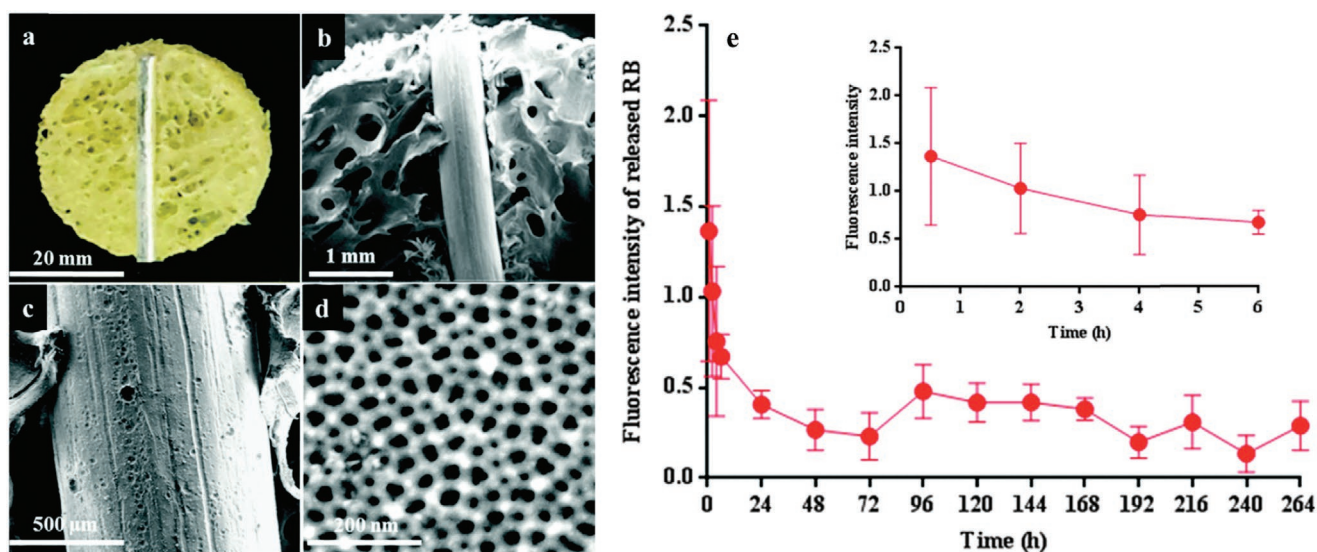


Figure 8. a) Digital image of the implant. b) SEM cross-section showing porous structure with implant. c,d) Homogenous surface morphology of NAA. e) Ex vivo drug elution kinetics from NAA implant (20.4 μm pore depth). Data represents mean and standard deviation from three replicates. Adapted with permission.^[72] Copyright 2015, Royal Society of Chemistry.

Table 2. Different types of modification procedures used for treatment of NAA.

Modification strategies	Materials/templates used	Summary	Refs.
Grafting	• Polyacrylic acid (PAA)	Hyperbranched structure excellent for covering the top of porous surface.	[74]
	• Poly(<i>N</i> -isopropylacrylamide) (PNIPAM)	Thermosensitive polymer widely known for its hydrophobic and hydrophilic switchable property at lower critical solution temperature.	[75,76]
	• Polystyrene sulfonate/poly- allylamine hydrochloride (PSS/PAH)	Easy modification along with high selectivity. Commonly used to entrap molecules inside nanopores effectively.	[49,77,78]
Chemical vapor deposition	• Carbon nanotube (CNT)/NAA composite	Excellent technique to control thickness of desired coated material as compared to other techniques.	[79,80,81,82,83]
	• NAA–carbon nanohybrid		
	• Chromium oxide (CrO ₂) nanowire arrays assisted by NAA		
	• Diamond-like carbon on NAA		
Thermal vapor deposition	• Platinum-coated NAA membranes	Simplest yet effective method used to improve chemical stability, conductivity, and magnetic properties.	[84,85,86]
	• Silver (Ag) nanocap arrays on NAA membrane		
Atomic layer deposition	• Iridium oxide (IrO ₂) deposition inside NAA	Can be used for sequential and conformational deposition of several materials with controlled thickness over the NAA surface.	[87,88,89]
	• Pt and Al ₂ O ₃ deposition on NAA membrane		
	• TiN–Al ₂ O ₃ –TiN composite inside NAA		
Silanization	• 3-aminopropyl trimethoxysilane (APTES)	Fast, effective, and reliable method to change the intrinsic as well as surface properties of NAA.	[90,91]
	• Octadecyltrimethoxysilane (ODS)		
Electrochemical deposition	• Palladium nanoparticles (Pd) on the surface of NAA	Widely used to deposit several metals or composites over NAA surfaces. Main advantage includes ease of use and excellent transfer of materials as compared to other deposition techniques.	[92,93,94]
	• Gold (Au) nanoparticles inside NAA		
	• Nickel (Ni) and cobalt (Co) nanowires into NAA		

aggregation of dextran molecules was formed inside the capsule resulting in larger molecular size. The study demonstrated successfully that drug release kinetics depends upon the size of drug molecules and can easily be altered by varying different pore sizes.

In a similar study, Jiang et al. in 2004 fabricated ultrathin alumina films on silicon to demonstrate the chip diffusion system. In this study, alumina membranes with a pore diameter of 40 nm and length of 1.2 μm were fabricated under 0.3 M oxalic acid at 40 V. To test diffusion experiments from alumina nanopores, caffeine, methyl orange (MO), and malachite green oxalate were used due to their ease of detection by optical absorbance. Molecular transport across the membranes was modeled using Fickian law and the diffusion coefficients were found to be $10^{-8} \text{ cm}^2 \text{ s}^{-1}$. In addition, a higher flux rate was observed for ultrathin membranes as compared to thick ones favoring for rapid transport of molecules from the pores.^[96]

Kipke and Schmid used commercially available NAA membranes with different pore sizes (20 and 50 nm) for the diffusion experiments of crystal violet molecules entrapped in micelles of sodium dodecylsulfate (SDS). Pore size was manipulated in order to get speed-controlled release from pores, which also served as a basis for novel drug delivery concepts. Due to low SDS concentration in the solution, the micelles were destroyed and crystal violet was released into the solution.^[97] Kwak et al. studied the influence of pore diameter and length of NAA on the release of the paclitaxel drug. The drug was loaded inside the pores by ultrasonication process whereas pore size was varied from 20 to 150 nm with the pore length of 2 μm . Using HPLC, it was shown that even after 400 h, the drug was releasing in a controlled manner. All the samples showed a similar release profile except ones with the smallest pore diameter (20–30 nm) due to the presence of most of the drug molecules on the surface. It was concluded that the drug

release does not depend on the pore diameter, but an increase in pore depth leads to a decrease in the amount of drug released from the structure.^[98]

In cardiology, to overcome the problem of restenosis, successful implantation of stents was performed by Sigwart et al. in 1987, which was helpful in reducing restenosis by 30%.^[99] However, after successful implantation of the stents, thrombotic aggregation and inflammatory reactions were observed in the tissue surrounding the injured site. To solve these problems, newly designed stents and coatings were applied on the stents to enhance biocompatibility and to deliver immunosuppressive drugs locally at the site.^[100] Among the coating agents, despite of clinical approval of several polymers^[101] due to delayed inflammation, other possibilities were also explored such as metal^[102] and ceramic coatings.^[103] In 2007, Kang et al. used NAA-coated stents for controlled drug release fabricated through anodization of Al on stents. In this study, the effect of different pore sizes and depth of NAA on drug release was studied through HPLC. It was shown that an increase in pore diameter leads to an increase in drug release rate whereas the increase in pore depth decreases the amount of drug being released from the pores.^[104] Similarly, Gultepe et al. reported the sustained release of DOX, an anticancer drug that was loaded onto NAA templates of different sizes (20 and 200 nm) and anodized titanium oxide templates (ATO, 125 nm). In situ measurements were obtained using a custom-made fluorometry setup and the intensity of DOX was measured with multiple readings taken without disturbing the setup. All of the release system used showed an extended release profile to the order of weeks. To remove the remaining drug from the pores, Tween 80 was used, and measurement was taken. Results were plotted using surface desorption model and it was proved that these types of systems are used for sustained drug release as an alternative to polymeric LDDS.^[105]

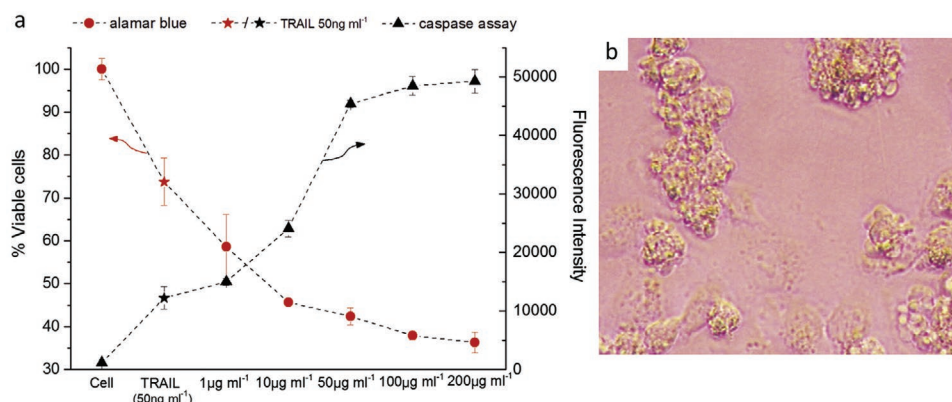


Figure 9. a) Drug release data from NAA-loaded Apo2L/TRAIL in PBS with Alamar blue and caspase assay after 165 min of treatment. b) Image depicts cell apoptosis due to NAA-loaded Apo2L/TRAIL at a concentration of 100 $\mu\text{g mL}^{-1}$ after treatment of 120 min. Black arrows depict NAATs in the media. Adapted with permission.^[70] Copyright 2014, Elsevier.

A new approach toward analysis of drug release was introduced by Kumeria et al. where the team demonstrated the real-time release of indomethacin drug from NAA templates using reflectometric interference spectroscopy (RIFS).^[106] The release measurements were performed in a microfluidic chip to demonstrate the drug elution in dynamic conditions. In brief, NAA was prepared using a two-step anodization process to obtain a pore diameter of 30–35 nm and length of 4.5 μm . Furthermore, these NAA implants were loaded with the drug and under varied flow rates (0, 10, 30, and 50 $\mu\text{L min}^{-1}$), release profiles were measured by a change in optical thickness with time using RIFS. In addition, a comparative profile of release was also obtained through conventional UV–visible (UV–vis) spectroscopy. The obtained results were fitted using the Higuchi model and it was shown that the drug release was directly proportional to flow rate, i.e., the higher the flow rate, the faster the release will be. As compared to traditional existing methods, RIFS system provides a more accurate and faster diffusion-controlled release analysis with the enhanced potential to be applied to several in vivo applications.

In a different approach, recently, Fazli-Abukheyli et al. covered the top of NAA surface with nanofibers of polyvinylidene fluoride/polyethylene glycol (PVDF/PEG) using an electrospinning approach to study the release of indole-3-acetic acid (IAA). Release measurements were obtained with drug-loaded NAA and a characteristically characteristic measurement of with and without nanofibers coating was exploited. The drug release behavior was explained by a two-stage process where the first stage was modeled by zero-order kinetics model and the second stage of release followed first order kinetics model. It was demonstrated that covering the NAA surface with nanofibers significantly decreases the burst release and increase the duration of release from the nanoporous template.^[107]

In recent years, different varieties of alumina nanoarchitectures were fabricated with the perspective of targeted DDS. In this regard, Lee et al. reported a novel method denominated as “pulse anodization” where both the MA and HA regimes were combined to obtain new 3D structures and membrane sheets.^[108] In brief, the procedure was performed using H_2SO_4 electrolyte where a low potential pulse was applied followed by

a high potential pulse in order to achieve MA and HA conditions, respectively.

Wang et al. reported the biocompatibility and cell uptake of NAAT and demonstrated their use as a potential carrier for delivery of Apo2L/TRAIL. In short, NAATs were fabricated by a modified galvanostatic method where a 5 s pulse was applied at a current density of 3 mA cm^{-2} followed by 2 s HA pulse of 350 mA cm^{-2} to obtain a pore size of 100 nm and length of 600 nm. Loading efficiency was calculated by thermogravimetric analysis with the capacity of 104 $\mu\text{g mg}^{-1}$, which is significantly higher as compared to other nanomaterials. It was observed during in vitro testing, that no burst release was seen but, around 40% of the drug was eluted after 30 min and thereafter sustained release profile was obtained for 240 min (Figure 9a). Cell apoptosis leads to a significant decrease in viability of MDA-MB231-TXSA after 165 min of incubation period with Apo2L/TRAIL-loaded NAATs (Figure 9b). The reason for such a decrease in viability was associated with an enhancement in caspase-3 activity, which was greater even at low doses of 1 $\mu\text{g mL}^{-1}$ of AANTs indicating that the apoptosis is from Apo2L/TRAIL eluting from AANTs. These findings proved that NAATs serves as an excellent carrier for drug delivery applications.^[70]

In relation, Porta-i-Batalla et al. from our group reported the impact of pore geometries on the release of drug from 3D nanostructures. In brief, different 3D structures (multi-layered nanofunnels (NFs) and inverted funnels (IFs), consisting of cylindrical pores with varied pore diameter) were fabricated (Figure 10). These structures were loaded with doxorubicin (1 mg mL^{-1}) and release profiles were analyzed using photoluminescence spectroscopy. Two different types of release were modeled by Higuchi (short-term) and Korsmeyer–Peppas (long-term) equations. Sustained drug elution profile for more than 60 days was achieved successfully without an initial burst release. It was shown that pore geometry impacted the release kinetics including the total amount of drug-loaded inside the pores (Figure 11a,b). In short-term release, release rates from inverted funnels were lower than straight pores (SPs) despite having the same pore diameter.^[37]

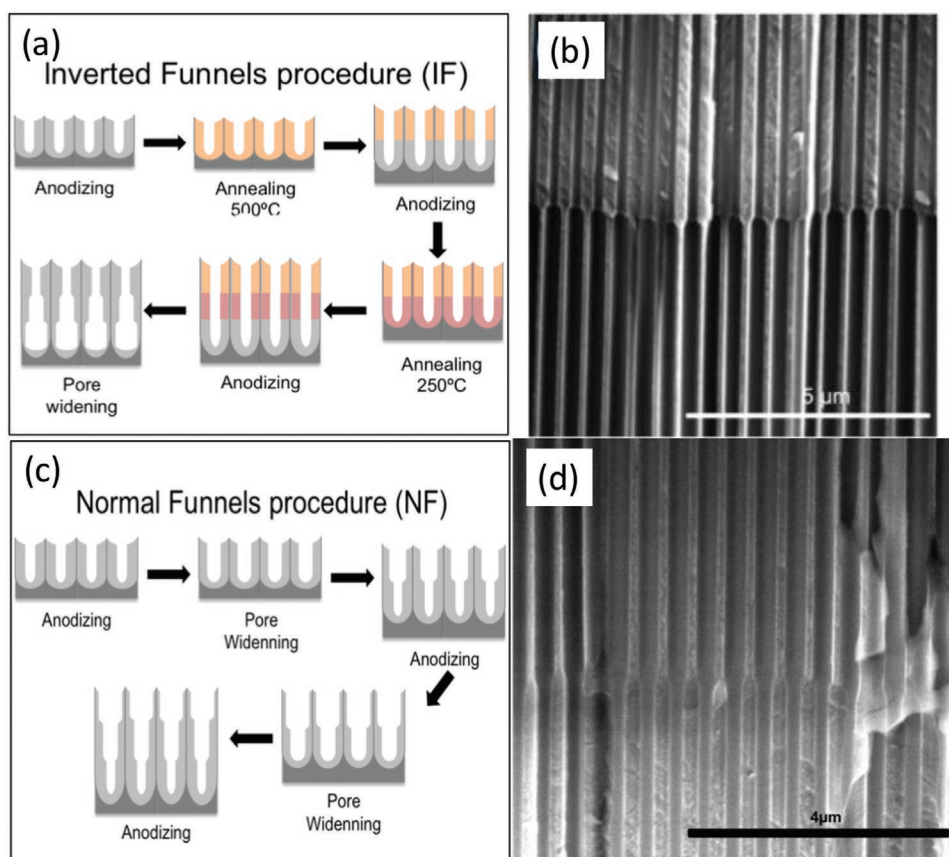


Figure 10. a) Schematic representation of fabrication of inverted funnels (IFs). b) Cross-section SEM image of IFs. c) Normal funnels (NFs) fabrication process. d) SEM cross-section of NFs. Adapted with permission.^[37] Copyright 2017, MDPI.

5. Stimuli-Based Strategies for Controlled Drug Release

Several protocols have been developed so far to release drugs in a controlled manner, but drug release still remains inconsistent

for a desired period of time. Therefore, to address the problem, new stimuli-based drug delivery systems based on NAA were introduced. Several stimuli (pH, temperature, magnetic field, light, and ultrasound) triggered drug delivery systems have recently gained enormous attention.^[8]

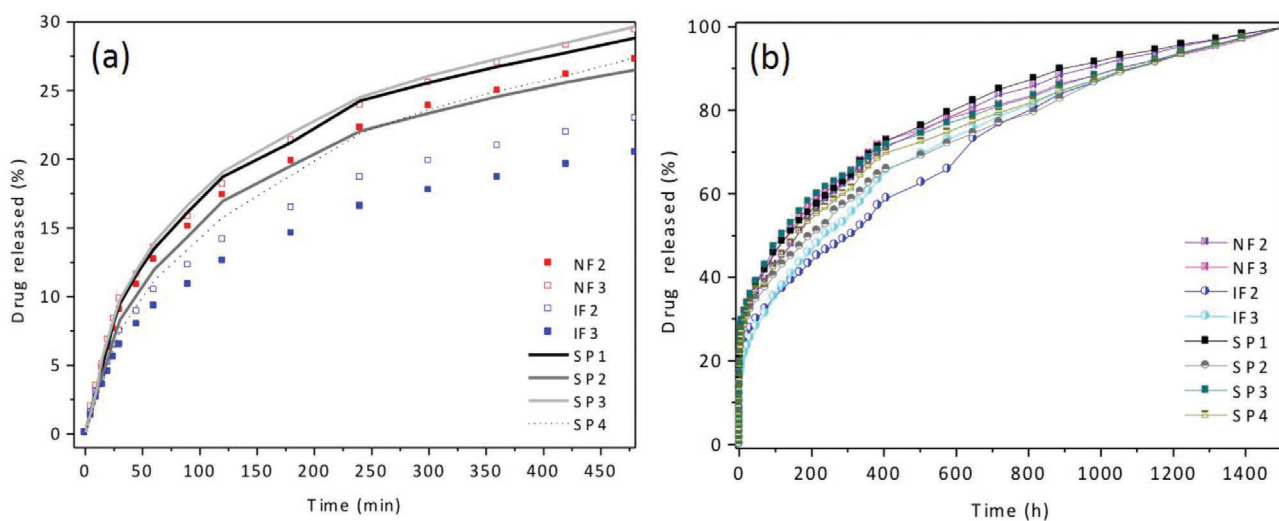


Figure 11. Cumulative drug release quantity obtained from photoluminescence spectra. a) Short-term and b) long-term for normal funnels (NFs), inverted funnels (IFs), and straight pores (SPs), respectively. Adapted with permission.^[37] Copyright 2017, MDPI.

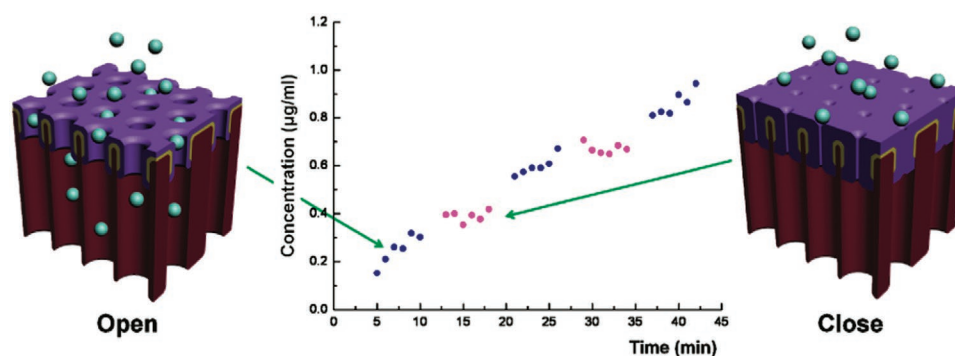


Figure 12. Schematic diagram of electrically responsive NAA membrane coated with PPy-DBS indicating reversible cycle of pore opening reduction (drug release) between oxidation and reduction states. Reprinted with permission.^[110] Copyright 2011, American Chemical Society.

Although there are several procedures to fabricate different types of nanoporous anodic structures, the process usually results in crystalline lattice defects, which promote nonspecific adhesion of several molecules on the surface leading to pore obstruction and biofouling. To overcome this challenge, Popat et al. reported the covalent modification of NAA surfaces with a pore size of 70 nm by polyethylene glycol (PEG) using PEG–silane chemistry. Different concentrations of PEG (10×10^{-3} , 20×10^{-3} , 40×10^{-3} , and 80×10^{-3} M) were used to demonstrate different grafting densities of polymer on NAA surfaces. The effect of different immobilization times (1, 2, 4, and 8 h) for 5×10^{-3} M concentration was studied. To check the nonfouling properties, unmodified and PEG-modified alumina surfaces were tested against fibrinogen (1 mg mL^{-1}) and all the results were confirmed using X-ray photoelectron spectroscopy. It was reported that the thickness of the film was less than 2.5 nm and thus, unable to clog the pores whereas with PEG-modified NAA surfaces 70% reduction in protein attachment was achieved.^[109]

Jeon et al. developed an electrically responsive drug delivery system based on the NAA membrane. In this study, electropolymerization was done on the top surface of NAA membranes using polypyrrole doped with dodecyl benzenesulfonate anion (PPy/DBS). The main idea was to actuate pore size electrically, by utilizing the drastic change in volume of PPy/DBS depending on the electrochemical state (Figure 12). The pore actuation was confirmed with AFM images and later, loaded with fluorescently labeled BSA. Apart from the fast switching time (less than 10 s), it was demonstrated that pores in the open state resulted in a high flux of drug from the NAA membrane which makes this system suitable for emergency treatment of diseases like migraine and angina pectoris.^[110]

In another study by Abelow et al., NAA membranes were coated with polypyrrole (PPy) and poly (3,4-ethylenedioxythiophene) (PEDOT) doped with chloride and *p*-toluene sulfonate (Tosylate) through vapor phase polymerization technique. Molecular diffusion rates of tannic acid were measured based on oxidation or reduction state of the polymer. It was shown that the diffusion through these polymer-coated nanostructures was faster when the polymer is in oxidation state while slower, being in the reduction state. The reason could be attributed to swelling/deswelling behavior along with the degree of confinement of polymer inside porous structure.^[111] Another

pioneering study performed by Kumeria et al., reported the controlled photoresponsive molecular transport of Rose Bengal (RosB) dye across the nanoporous anodic alumina membranes (NAAM) using photoswitchable peptide (PSP). In this study, an azobenzene-derived peptide was immobilized along the internal part of 3-aminopropyl trimethoxysilane (APTES)-modified nanoporous channel for a change in effective pore diameter of the structure and subsequently, tracking the movement of dye molecules using a change in *cis/trans* configuration of the peptide. The NAAM/PSP structure was first treated with light with a wavelength of 400 nm for a duration of 60 min, which resulted in low molecular transport, however, when the exposure was changed to 364 nm, an increasing trend was observed in the dye concentration due to change in the isomeric property. It was shown that exposing the structure to 364 nm wavelength leads to reversible switching in azobenzene structure from *trans* to *cis* isomer.^[112]

Noh utilized NAA nanotubes as a drug delivery reservoir for the widely used antibiotic Amoxicillin ($\approx 8 \text{ nm}$). With the unique geometrical features of fabricated NAA, i.e., almost similar pore size and spacing between the neighboring nanotubes (20 nm) and height of $38 \mu\text{m}$, sustained release was observed for nearly 5 weeks. It was shown that the drug released from the pores was proportional to the square root of time calculated using the Higuchi model.^[50] In a similar study, Controlled release profile of another antibiotic, vancomycin, was achieved by Simovic et al. where NAA was decorated with biopolymer coating to reduce pore opening and closing. In this approach, the plasma polymerization tool was used to deposit a thin layer of polyallylamine on the top part of NAA, thereby reducing the pore size by 5 nm (Figure 13a,b). Three different time periods (50, 120, and 200 s) of polyallylamine were deposited and release was compared against samples without polymer deposition. It was shown that an increase in the deposition period of the polymer diminishes the drug release. On one hand, where uncoated NAA samples eluted the drug within 45 min, the deposition of 50 s extended the release for up to 200 h, whereas for 120 s deposition, the release time period was increased to 500 h. Concerning the final deposition period, i.e., 200 s, within 500 h, only half of the drug was released thus giving the possibility to tune pore size and in turn controlling the drug release. Zero-order release was obtained after fitting the data into zero-order

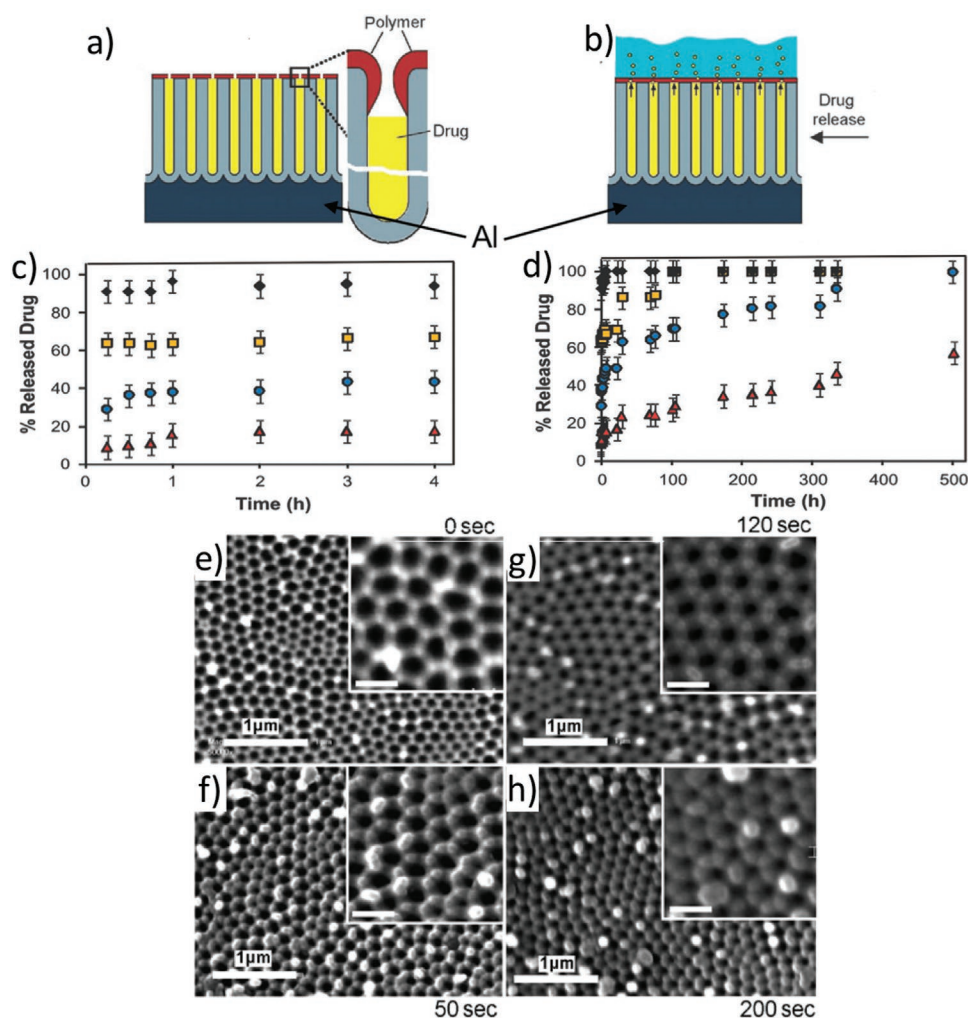


Figure 13. a) Schematic demonstrating the decrease in pore opening of NAA by deposition of polyallylamine using plasma polymerization tool. b) Diffusion of vancomycin from modified nanotube arrays into PBS medium. c,d) Controlled release profile of vancomycin from NAA without deposition and with controlled deposition time of 50 s (squares), 120 s (circles), and 200 s (triangles) for 4 and 500 h, respectively. e) SEM images without deposition of polyallylamine and f–h) with deposition time of 50, 200, and 300 s, respectively. Adapted with permission.^[113] Copyright 2010, Royal Society of Chemistry.

equation (Figure 13c,d). SEM images have been shown in Figure 13e–h without depositing polyallylamine and after the deposition time of 50, 200, and 300 s respectively.^[113]

Recently, Porta-i-Batalla et al. from our group reported stimuli-driven drug delivery system using pH-responsive polyelectrolytes and NAA as a template. Drug release kinetics were evaluated based on a change in pH and the number of polyelectrolyte layers.^[49] In brief, NAA was fabricated with two-step electrochemical anodization with a pore size of 130 nm and depth of 15 μm. These uniform NAA structures were dipped alternatively in a solution of negative poly(styrene sulfonate) (PAS) and positive poly(allylamine hydrochloride) (PAH) to get two, five, and eight layers, respectively (Figure 14a–h). The dipping time of NAA in both the electrolytes was set to 30 min followed by 10 min of rinsing in deionized water. Doxorubicin (DOX) was chosen as a model drug for this study. Polyelectrolyte-coated samples were placed in 1 mg mL^{−1} of DOX solution and the pH were adjusted to 2.0 to increase the permeability

of polyelectrolytes layers and for the fusion of DOX molecules inside PSS/PAH layers. Afterward, pH was changed to 8.0 to cause contraction of the polyelectrolyte multilayers, which results in entrapment of drug molecules inside the films. Drug release profile was measured using photoluminescence spectroscopy in two different pH medium 5.2 and 7.4 for over 5 days (Figure 15). It was demonstrated that at acidic pH, DOX released at a faster rate and was found to be in correlation with the number of polyelectrolyte bilayers. On the other hand, at alkaline pH the drug release kinetics were not linear with the number of polyelectrolytes bilayers which suggests that only the drug located near to the release medium was released. To test the pH responsiveness of the system, a sudden change of pH was performed during the release which led to another burst release confirming the same.

Zhao et al. recently developed a dual stimuli (pH and temperature) NAA membrane for controlled drug release of dexamethasone.^[114] In this study, NAA membranes were

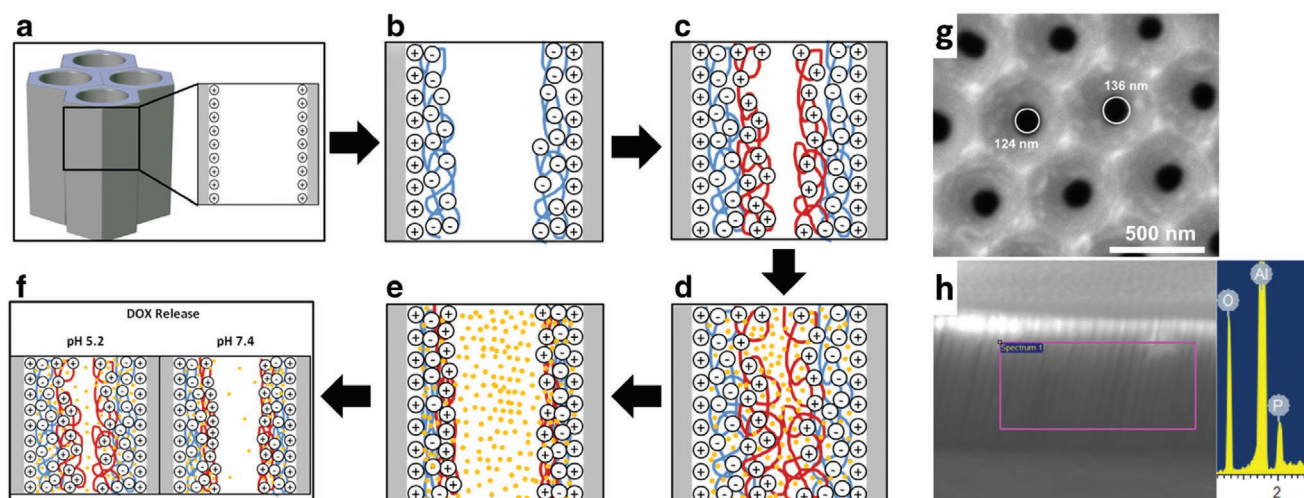


Figure 14. Schematic visualization of polyelectrolytes deposition in NAA structures. a) NAA pore walls were coated with positively charged APTES molecules. b) Deposition of negative PSS layer. c) PSS-coated NAA were dipped in PAH solution to get positive layer. d) At pH 2.0, DOX loading into swollen multilayers. e) Confinement of DOX molecules due to contraction at pH 8.0. f) Release of drug molecules at different pH (5.2 and 7.4). g) SEM image of NAA pore diameter. h) Cross-sectional image of NAA with EDX spectra confirming polyelectrolyte deposition. Adapted with permission.^[49] Copyright 2016, Springer.

fabricated by two-step anodization in which the first part was coated with biocompatible colipid and the remaining part was used for drug loading. To verify the different parts, FITC was coated selectively onto APTES-modified NAA and observed with laser scanning confocal microscopy (LSCM). The electrochemical behavior of as-prepared NAA membranes was tested for pH responsiveness and temperature dependency using the voltammetry technique. The drug release measurement was performed using UV-vis under different pH conditions (5.2, 6.4, and 7.4) and different temperatures (25, 35, 40, and 50 °C). It was found that there was an increase in drug elution kinetics of about fourfold to sixfold at acidic pH and high temperature (50 °C). To investigate the versatility of the PAA membrane, another anticancer drug (doxorubicin) was tested. No significant differences were found between the

drug release kinetics of both the drugs, with higher release efficiency at pH 5.2 as compared to neutral pH (7.4).

6. Conclusion and Future Perspective

This review highlights the recent advances and breakthrough structural engineering of NAA for drug delivery applications. This material has gained enormous attention in the scientific community already due to its unique properties, scalable, and low-cost production. It has already been proved that homogenous pore distribution, high surface area-to-volume ratio, tunability, stable physiochemical stability, and excellent mechanical strength renders this material to be widely used in biomedical applications. Furthermore, NAA can strictly be tailored to trigger an enhanced response from the delivery systems. Integrating this material with appropriate chemistry to interact with the biological elements can be helpful in early diagnosis and treatment of several diseases.

This review has proved that there is still plenty of room for advance and growth in applications for this material. More emphasis can be given on the modified anodization procedures and stable chemistries to enhance the drug loading inside NAA. We have already summarized the successful use of NAA in several biomedical applications, i.e., cardiology, tissue engineering, etc. To conclude, more research efforts should be focused on exploring new NAA architectures, chemical modifications and making them biocompatible enough to deliver therapeutics effectively and harmlessly to the targeted site. In addition, more medications like antineoplastic, anesthetic, antipyretic, antithrombotic, and many more agents need to be tested with these architectures to achieve successful drug delivery platforms. Future developments should be redirected for more in vivo studies with the research already published to make NAA as widely acceptable material for clinical applications. These might include integrating them with sensors, micro and nanochips, lab-on-a-chip technology for sustained drug delivery.

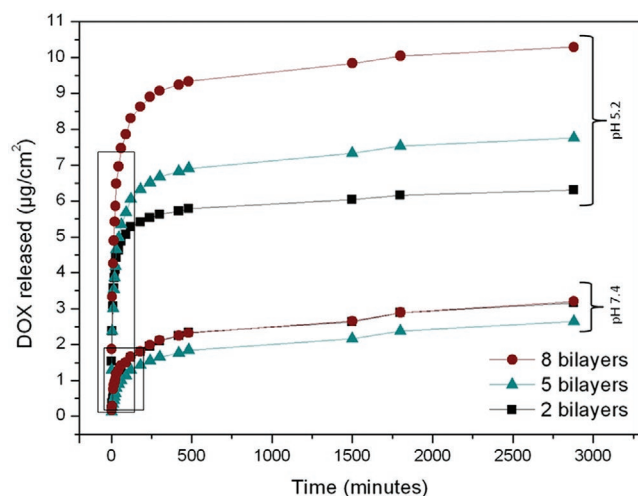


Figure 15. Drug release kinetics from NAA coated with different polyelectrolyte layers at different pH (5.2 and 7.4) with two different burst release shown. Adapted with permission.^[49] Copyright 2016, Springer.

Acknowledgements

This work was partially supported by the Spanish Ministerio de Ciencia, Innovación y Universidades (MICINN/FEDER) RTI2018-094040-B-I00, the Agency for Management of University and Research Grants (AGAUR) Ref. 2017-SGR-1527, and the Catalan Institution for Research and Advanced Studies (ICREA) under the ICREA Academia Award.

Conflict of Interest

The authors declare no conflict of interest.

Keywords

drug delivery, electrochemical anodization, nanoporous anodic alumina

Received: June 26, 2020

Revised: August 14, 2020

Published online:

- [1] Y. H. Yun, B. K. Lee, K. Park, *J. Controlled Release* **2015**, 219, 2.
- [2] J. Folkman, D. M. Long, R. Rosenbaum, *Science* **1966**, 154, 148.
- [3] A. S. Hoffman, *J. Controlled Release* **2008**, 132, 153.
- [4] K. K. Jain, *Methods Mol. Biol.* **2008**, 437, 1.
- [5] J. Cannon, *Drug Delivery Systems*, 3rd ed., CRC Press, Boca Raton, FL **2011**.
- [6] R. Mainardes, L. Silva, *Curr. Drug Targets* **2004**, 5, 449.
- [7] D. A. LaVan, T. McGuire, R. Langer, *Nat. Biotechnol.* **2003**, 21, 1184.
- [8] A. Santos, M. Sinn Aw, M. Bariana, T. Kumeria, Y. Wang, D. Losic, *J. Mater. Chem. B* **2014**, 2, 6157.
- [9] K. Madaan, S. Kumar, N. Poonia, V. Lather, D. Pandita, *J. Pharm. BioAllied Sci.* **2014**, 6, 139.
- [10] E. Calzoni, A. Cesaretti, A. Polchi, A. Di Michele, B. Tancini, C. Emiliani, *J. Funct. Biomater.* **2019**, 10, 4.
- [11] J. Liu, L. Cui, D. Losic, *Acta Biomater.* **2013**, 9, 9243.
- [12] J. B. Wolinsky, Y. L. Colson, M. W. Grinstaff, *J. Controlled Release* **2012**, 159, 14.
- [13] J. Ferré-Borrull, J. Pallarès, G. Macías, L. F. Marsal, *Materials* **2014**, 7, 5225.
- [14] A. Santos, J. Ferré-Borrull, J. Pallarès, L. F. Marsal, *Phys. Status Solidi* **2011**, 208, 668.
- [15] M. Alba, P. Formentín, J. Ferré-Borrull, J. Pallarès, L. F. Marsal, *Nanoscale Res. Lett.* **2014**, 9, 411.
- [16] K. Gulati, S. Ramakrishnan, M. S. Aw, G. J. Atkins, D. M. Findlay, D. Losic, *Acta Biomater.* **2012**, 8, 449.
- [17] A. Santos, P. Formentín, J. Pallarès, J. Ferré-Borrull, L. F. Marsal, *J. Electroanal. Chem.* **2011**, 655, 73.
- [18] E. Xifre-Perez, S. Guaita-Esteruelas, M. Baranowska, J. Pallares, L. Masana, L. F. Marsal, *ACS Appl. Mater. Interfaces* **2015**, 7, 18600.
- [19] C. Eckstein, L. K. Acosta, L. Pol, E. Xifré-Pérez, J. Pallares, J. Ferré-Borrull, L. F. Marsal, *ACS Appl. Mater. Interfaces* **2018**, 10, 10571.
- [20] L. Pol, C. Eckstein, L. K. Acosta, E. Xifré-Pérez, J. Ferré-Borrull, L. F. Marsal, *Nanomaterials* **2019**, 9, 478.
- [21] M. Amouzadeh Tabrizi, J. Ferré-Borrull, L. F. Marsal, *Biosens. Bioelectron.* **2019**, 137, 279.
- [22] L. K. Acosta, F. Bertó-Roselló, E. Xifre-Perez, A. Santos, J. Ferré-Borrull, L. F. Marsal, *ACS Appl. Mater. Interfaces* **2019**, 11, 3360.
- [23] V. S. Balderrama, J. Albero, P. Granero, J. Ferré-Borrull, J. Pallarès, E. Palomares, L. F. Marsal, *Nanoscale* **2015**, 7, 13848.
- [24] M. A. Tabrizi, J. Ferré-Borrull, P. Kapruwan, L. F. Marsal, *Microchim. Acta* **2019**, 186, 117.
- [25] M. A. Tabrizi, J. Ferré-Borrull, L. F. Marsal, *Sens. Actuators, B* **2019**, 304, 127302.
- [26] W. Lee, S.-J. Park, *Chem. Rev.* **2014**, 114, 7487.
- [27] H. Masuda, K. Fukuda, *Science* **1995**, 268, 1466.
- [28] H. Masuda, *J. Electrochem. Soc.* **1997**, 144, L127.
- [29] A. P. Li, F. Müller, A. Bimer, K. Nielsch, U. Gösele, *J. Appl. Phys.* **1998**, 84, 6023.
- [30] S. Ono, M. Saito, H. Asoh, *Electrochim. Acta* **2005**, 51, 827.
- [31] S. Ono, M. Saito, M. Ishiguro, H. Asoh, *J. Electrochem. Soc.* **2004**, 151, B473.
- [32] W. Lee, R. Ji, U. Gösele, K. Nielsch, *Nat. Mater.* **2006**, 5, 741.
- [33] A. Santos, *J. Mater. Chem. C* **2017**, 5, 5581.
- [34] W. Lee, R. Scholz, U. Gösele, *Nano Lett.* **2008**, 8, 2155.
- [35] Y. Wang, G. Kaur, A. Zysk, V. Liapis, S. Hay, A. Santos, D. Losic, A. Evdokiou, *Biomaterials* **2015**, 46, 117.
- [36] J. T. Domagalski, E. Xifre-Perez, A. Santos, J. Ferré-Borrull, L. F. Marsal, *Microporous Mesoporous Mater.* **2020**, 303, 110264.
- [37] M. Porta-i-Batalla, E. Xifré-Pérez, C. Eckstein, J. Ferré-Borrull, L. F. Marsal, *Nanomaterials* **2017**, 7, 227.
- [38] T. Nagaura, F. Takeuchi, S. Inoue, *Electrochim. Acta* **2008**, 53, 2109.
- [39] C. S. Law, S. Y. Lim, A. Santos, *Sci. Rep.* **2018**, 8, 4642.
- [40] C. S. Law, L. F. Marsal, A. Santos, *Handbook of Nanomaterials in Analytical Chemistry: Modern Trends in Analysis*, Elsevier, Amsterdam **2019**, pp. 201–226.
- [41] C. S. Law, S. Y. Lim, L. Liu, A. D. Abell, L. F. Marsal, A. Santos, *Nanoscale* **2020**, 12, 9404.
- [42] C. S. Law, S. Y. Lim, A. D. Abell, L. F. Marsal, A. Santos, *Nanoscale* **2018**, 10, 14139.
- [43] D. Li, L. Zhao, C. Jiang, J. G. Lu, *Nano Lett.* **2010**, 10, 2766.
- [44] D. Losic, M. Lillo, *Small* **2009**, 5, 1392.
- [45] K. Schwirn, W. Lee, R. Hillebrand, M. Steinhart, K. Nielsch, U. Gösele, *ACS Nano* **2008**, 2, 302.
- [46] D. Losic, S. Simovic, *Expert Opin. Drug Delivery* **2009**, 6, 1363.
- [47] P. Roy, S. Berger, P. Schmuki, *Angew. Chem., Int. Ed.* **2011**, 50, 2904.
- [48] M. Sinn Aw, M. Kurian, D. Losic, *Biomater. Sci.* **2014**, 2, 10.
- [49] M. Porta-i-Batalla, C. Eckstein, E. Xifré-Pérez, P. Formentín, J. Ferré-Borrull, L. F. Marsal, *Nanoscale Res. Lett.* **2016**, 11, 372.
- [50] K. Noh, *J. Biomater. Nanobiotechnol.* **2011**, 02, 226.
- [51] J. M. Morais, F. Papadimitrakopoulos, D. J. Burgess, *AAPS J.* **2010**, 12, 188.
- [52] R. Trindade, T. Albrektsson, P. Tengvall, A. Wennerberg, *Clin. Implant Dent. Relat. Res.* **2016**, 18, 192.
- [53] M. S. Aw, D. Losic, *Intelligent Nanomaterials*, 2nd ed., John Wiley & Sons, Inc., Hoboken, NJ **2016**, pp. 127–159.
- [54] F. Haq, V. Anandan, C. Keith, G. Zhang, *Int. J. Nanomed.* **2007**, 2, 107.
- [55] E. P. Briggs, A. R. Walpole, P. R. Wilshaw, M. Karlsson, E. Pålsgård, *J. Mater. Sci.: Mater. Med.* **2004**, 15, 1021.
- [56] B. Wolfrum, Y. Mourzina, F. Sommerhage, A. Offenhäusser, *Nano Lett.* **2006**, 6, 453.
- [57] T. Ishibashi, Y. Hoshino, H. Kaji, M. Kanzaki, M. Sato, M. Nishizawa, *Biomed. Microdevices* **2009**, 11, 413.
- [58] M. Karlsson, L. Tang, *J. Mater. Sci.: Mater. Med.* **2006**, 17, 1101.
- [59] M. Baranowska, A. J. Slota, P. J. Eravuchira, G. Macias, E. Xifré-Pérez, J. Pallares, J. Ferré-Borrull, L. F. Marsal, *Colloids Surf., B* **2014**, 122, 375.
- [60] S. Bose, J. Darsell, H. L. Hosick, L. Yang, D. K. Sarkar, A. Bandyopadhyay, *J. Mater. Sci.: Mater. Med.* **2002**, 13, 23.
- [61] K. E. Orosz, S. Gupta, M. Hassink, M. Abdel-Rahman, L. Moldovan, F. H. Davidorf, N. I. Moldovan, *Mol. Vision* **2004**, 10, 555.
- [62] K. E. La Flamme, G. Mor, D. Gong, T. La Tempa, V. A. Fusaro, C. A. Grimes, T. A. Desai, *Diabetes Technol. Ther.* **2005**, 7, 684.
- [63] T. A. Desai, W. H. Chu, G. Rasi, P. Sinibaldi-Vallebona, E. Guarino, M. Ferrari, *Biomed. Microdevices* **1999**, 1, 131.

- [64] S. Pujari-Palmer, T. Lind, W. Xia, L. Tang, M. Karlsson Ott, J. Biomater. Nanobiotechnol. **2014**, 05, 98.
- [65] A. R. Walpole, E. P. Briggs, M. Karlsson, E. Pålsgård, P. R. Wilshaw, Materialwiss. Werkstofftech. **2003**, 34, 1064.
- [66] A. Friedmann, A. Hoess, A. Cismak, A. Heilmann, Acta Biomater. **2011**, 7, 2499.
- [67] G. E. J. Poinern, X. T. Le, M. O'Dea, T. Becker, D. Fawcett, BioMed Res. Int. **2014**, 2014, 238762.
- [68] S. Ni, C. Li, S. Ni, T. Chen, T. J. Webster, Int. J. Nanomed. **2014**, 9, 3325.
- [69] S. Thakur, S. Massou, A. M. Benoliel, P. Bongrand, M. Hanbucken, K. Sengupta, Nanotechnology **2012**, 23, 255101.
- [70] Y. Wang, A. Santos, G. Kaur, A. Evdokiou, D. Losic, Biomaterials **2014**, 35, 5517.
- [71] H. Wienieke, O. Dirsch, T. Sawitowski, Y. L. Gu, H. Brauer, U. Dahmen, A. Fischer, S. Wnendt, R. Erbel, Catheter Cardiovasc. Interventions **2003**, 60, 399.
- [72] S. Rahman, G. J. Atkins, D. M. Findlay, D. Losic, J. Mater. Chem. B **2015**, 3, 3288.
- [73] C. Y. Han, G. A. Willing, Z. Xiao, H. H. Wang, Langmuir **2007**, 23, 1564.
- [74] M. Nagale, B. Y. Kim, M. L. Bruening, J. Am. Chem. Soc. **2000**, 122, 11670.
- [75] P. F. Li, R. Xie, J. C. Jiang, T. Meng, M. Yang, X. J. Ju, L. Yang, L. Y. Chu, J. Membr. Sci. **2009**, 337, 310.
- [76] H. J. Wang, W. H. Zhou, X. F. Yin, Z. X. Zhuang, H. H. Yang, X. R. Wang, J. Am. Chem. Soc. **2006**, 128, 15954.
- [77] J. Dai, G. L. Baker, M. L. Bruening, Anal. Chem. **2006**, 78, 135.
- [78] F. S. H. Krismastuti, H. Bayat, N. H. Voelcker, H. Schönherr, Anal. Chem. **2015**, 87, 3856.
- [79] A. Popp, J. Engstler, J. J. Schneider, Carbon **2009**, 47, 3208.
- [80] K. Rana, G. Kucukayan-Dogu, E. Bengu, Appl. Surf. Sci. **2012**, 258, 7112.
- [81] J. Fang, I. Levchenko, T. Van Der Laan, S. Kumar, K. Ostrikov, Carbon **2014**, 78, 627.
- [82] Q. Zhao, G. Wen, Z. Liu, Y. Fan, G. Zou, L. Li, R. Zheng, S. P. Ringer, H. K. Mao, Nanotechnology **2011**, 22, 125603.
- [83] M. Aramesh, K. Fox, D. W. M. Lau, J. Fang, K. Ostrikov, S. Praver, J. Cervenka, Carbon **2014**, 75, 452.
- [84] P. S. Cheow, E. Z. C. Ting, M. Q. Tan, C. S. Toh, Electrochim. Acta **2008**, 53, 4669.
- [85] B. T. T. Nguyen, E. Z. C. Ting, C. S. Toh, Bioinspiration Biomimetics **2008**, 3, 035008.
- [86] T. Qiu, W. Zhang, X. Lang, Y. Zhou, T. Cui, P. K. Chu, Small **2009**, 5, 2333.
- [87] D. J. Comstock, S. T. Christensen, J. W. Elam, M. J. Pellin, M. C. Hersam, Electrochem. Commun. **2010**, 12, 1543.
- [88] G. Pardon, H. K. Gatty, G. Stemme, W. van der Wijngaart, N. Roxhed, Nanotechnology **2013**, 24, 015602.
- [89] K. Pitzschel, J. M. M. Moreno, J. Escrig, O. Albrecht, K. Nielsch, J. Bachmann, ACS Nano **2009**, 3, 3463.
- [90] D. J. Odom, L. A. Baker, C. R. Martin, J. Phys. Chem. B **2005**, 109, 20887.
- [91] A. Mutalib Md Jani, E. J. Anglin, S. J. P. McInnes, D. Losic, J. G. Shapter, N. H. Voelcker, Chem. Commun. **2009**, 3062.
- [92] M. Platt, R. A. W. Dryfe, E. P. L. Roberts, Electrochim. Acta **2003**, 48, 3037.
- [93] T. Kondo, K. Nishio, H. Masuda, Appl. Phys. Express **2009**, 2, 032001.
- [94] T. M. Whitney, J. S. Jiang, P. C. Searson, C. L. Chien, Science **1993**, 261, 1316.
- [95] D. Gong, V. Yadavalli, M. Paulose, M. Pishko, C. A. Grimes, Biomed. Microdevices **2003**, 5, 75.
- [96] X. Jiang, N. Mishra, J. N. Turner, M. G. Spencer, Microfluid. Nano-fluid. **2008**, 5, 695.
- [97] S. Kipke, G. Schmid, Adv. Funct. Mater. **2004**, 14, 1184.
- [98] D.-H. Kwak, J.-B. Yoo, D. J. Kim, J. Nanosci. Nanotechnol. **2010**, 10, 345.
- [99] U. Sigwart, J. Puel, V. Mirkovitch, F. Joffe, L. Kappenberger, N. Engl. J. Med. **1987**, 316, 701.
- [100] G. E. Park, T. J. Webster, J. Biomed. Nanotechnol. **2006**, 1, 18.
- [101] W. J. van der Giessen, C. J. Slager, H. M. van Beusekom, D. S. van Ingen Schenau, R. A. Huijts, J. C. Schuurbers, W. J. de Klein, P. W. Serruys, P. D. Verdouw, J. Interventional Cardiol. **1992**, 5, 175.
- [102] C. Hehrlein, M. Zimmermann, J. Metz, W. Ensinger, W. Kübler, Coron. Artery Dis. **1995**, 6, 581.
- [103] H. Wienieke, T. Sawitowski, S. Wnendt, A. Fischer, O. Dirsch, I. A. Karoussos, R. Erbel, Herz **2002**, 27, 518.
- [104] H. J. Kang, D. J. Kim, S. J. Park, J. B. Yoo, Y. S. Ryu, Thin Solid Films **2007**, 515, 5184.
- [105] E. Gultepe, D. Nagesha, B. D. F. Casse, R. Banyal, T. Fitchorov, A. Karma, M. Amiji, S. Sridhar, Small **2010**, 6, 213.
- [106] T. Kumeria, K. Gulati, A. Santos, D. Losic, ACS Appl. Mater. Interfaces **2013**, 5, 5436.
- [107] R. Fazli-Abukheyli, M. R. Rahimi, M. Ghaedi, J. Drug Delivery Sci. Technol. **2019**, 54, 101247.
- [108] W. Lee, K. Schwirn, M. Steinhart, E. Pippel, R. Scholz, U. Gösele, Nat. Nanotechnol. **2008**, 3, 234.
- [109] K. C. Papat, G. Mor, C. A. Grimes, T. A. Desai, Langmuir **2004**, 20, 8035.
- [110] G. Jeon, S. Y. Yang, J. Byun, J. K. Kim, Nano Lett. **2011**, 11, 1284.
- [111] A. E. Abelow, K. M. Persson, E. W. H. Jager, M. Berggren, I. Zharov, Macromol. Mater. Eng. **2014**, 299, 190.
- [112] T. Kumeria, J. Yu, M. Alsawat, M. D. Kurkuri, A. Santos, A. D. Abell, D. Losic, Adv. Mater. **2015**, 27, 3019.
- [113] S. Simovic, D. Losic, K. Vasilev, Chem. Commun. **2010**, 46, 1317.
- [114] X. P. Zhao, S. S. Wang, M. R. Younis, X. H. Xia, C. Wang, Adv. Mater. Interfaces **2018**, 5, 1800185.



Pankaj Kapruwan is a Ph.D. student at Universitat Rovira i Virgili, Campus Sescelades, Tarragona, Spain. He finished his dual master degrees (M.Sc. + M.Tech) in Nanoscience by Research and Nanotechnology at Amity University (2015) in India. He obtained Marti-Franques research scholarship in 2018 and started working at Departamento de Ingeniería Electrónica, Eléctrica y Automática, Universitat Rovira i Virgili. Currently, his research focuses on fabrication of different nanoporous anodic alumina structures with special emphasis on controlled drug release.



Josep Ferré-Borrull obtained his Physics degree in 1994, his B.Sc. in 1996, and his Ph.D. in 1998, all of them at the Universitat de Barcelona. His doctoral thesis was in the field of optical image processing. His postdoctoral experience was focused on the characterization of nanoroughness of surfaces in high-quality optical components in the Fraunhofer Institute in Jena, Germany, and in the ENEA in Rome, Italy. Since he joined the Universitat Rovira i Virgili in 2004, he has been involved in research on the framework of the activities of the Nanoelectronic and Photonics group: development of technologies for the fabrication of nanoporous materials and their applications to energy, health, and environment, and especially in the numerical modeling of the interaction of light with such materials and devices.



Lluís F. Marsal is a full professor and distinguished professor at the Department of Electronic, Electrical and Automatic Engineering of the Universitat Rovira i Virgili, Spain. He obtained his Ph.D. degree in Physics in 1997 from the Universitat Politècnica de Catalunya, Spain. He was a postdoctoral researcher at the Department of Electrical and Computer Engineering, University of Waterloo, Ontario, Canada (1998–99). He is a senior member of the Institute of Electrical and Electronics Engineers and of the Optical Society of America. Dr. Marsal is a distinguished lecturer of the Electron Devices Society. His current research interests include nanophotonics, biosensors, and drug delivery based on porous materials and organic and hybrid nanostructured materials for optoelectronic devices.